0026-895X/11/8003-434–445$25.00
MOLECULAR PHARMACOLOGY
Copyright © 2011 The American Society for Pharmacology and Experimental Therapeutics
*Mol Pharmacol* 80:434–445, 2011

Vol. 80, No. 3
73403/3712475
*Printed in U.S.A.*



# A Dynamic Model of Membrane-Bound Phospholipase Cβ2 Activation by Gβγ Subunits

Daniel S. Han, Urszula Golebiewska, Sebastian Stolzenberg, Suzanne F. Scarlata, and Harel Weinstein

*Department of Physiology and Biophysics, Weill Cornell Medical College, Cornell University, New York, New York (D.H., S.S., H.W.); and Department of Physiology & Biophysics, Stony Brook University, Stony Brook, New York (U.G., S.F.S.)*

Received May 6, 2011; accepted June 20, 2011

## ABSTRACT

Phospholipase C (PLC) β2, a well studied member of the family of enzymes that catalyze the hydrolysis of the membrane lipid phosphatidylinositol 4,5-bisphosphate ($PIP_2$) into secondary messengers, can be activated by the Gβγ subunits of heterotrimeric G-proteins in a manner that depends on the presence and composition of the associated phospholipid membrane surface. The N-terminal pleckstrin homology (PH) domain of PLCβ2 mediates both the response to Gβγ and membrane binding, but how these interactions are coupled to yield an activated catalytic core remains unknown. Here we propose a mechanism based on molecular models of truncated PLCβ2 in its activated form complexed with Gβγ and in the catalytically inactive/membrane-bound form, obtained with the application of protein-protein docking algorithms and coarse-grained molecular dynamics simulations. These models were probed experimentally, and the inferences were confirmed by results from a combination of molecular biology and fluorescence assays. Results from the dynamic simulations of the molecular models and their interactions with various lipid bilayers identify the determinants of PLCβ2-PH domain specificity for Gβγ and lipid membranes and suggest a mechanism for the previously reported dependence of Gβγ activation on the associated membrane composition. Together, these findings explain the roles of the different activators in terms of their effect on the orientations of the PH and catalytic core domains relative to the lipid membranes.





## Introduction

Mammalian phospholipase C (PLC) enzymes are multidomain proteins that catalyze the hydrolysis of phosphatidylinositol 4,5-bisphosphate ($PIP_2$) to generate the second messengers inositol 1,4,5-trisphosphate and diacylglycerol (Suh et al., 2008). In addition to the catalytic domain, PLCs contain multiple regulatory protein domains (Rebecchi and Pentyala, 2000; Rhee, 2001). Members of the PLCβ family contain a pleckstrin homology (PH) domain, an "EF hand" domain, the X-Y catalytic (CAT) domain, a C2 domain, and a coiled-coiled helical C-terminal region. Each domain is known to interact with other proteins, phospholipids, and ions with varying affinities within the PLC family, and these interactions ultimately serve to regulate the physiological activity of the protein (Drin and Scarlata, 2007). The PH domains play a particularly important role in the regulation of PLCβ2 by mediating both protein activators (Harden and Sondek, 2006; Drin and Scarlata, 2007) and membrane association (Wang et al., 1999).

Rac1 and Gβγ regulate PLCβ2. Based on recent crystal structures of PLCβ2 constructs (Jezyk et al., 2006; Hicks et al., 2008), the activating interaction with Rac1 was considered to occur exclusively through the PH domain. These studies suggested that Rac1 activates PLCβ2 by stabilizing its membrane association, which in turn destabilizes the association of a negatively charged loop to the catalytic region.

Activation of PLCβ2 by Gβγ subunits occurs by a mechanism that is distinct from Rac1, because the Rac1-activated

This work was supported by the National Institutes of Health National Institutes on Drug Abuse [Grants P01-DA012408, P01-DA012923, T32-DA007274]; and the National Institutes of Health National Institutes of General Medical Sciences [Grant R01-GM053132].

Article, publication date, and citation information can be found at http://molpharm.aspetjournals.org.

doi:10.1124/mol.111.073403.

**ABBREVIATIONS:** PLC, mammalian inositol-specific phospholipase C; PH, pleckstrin homology; CAT, catalytic; POPC, 1-palmitoyl-2-oleoyl-*sn*-glycero-3-phosphocholine; POPE, 1-palmitoyl-2-oleoyl-*sn*-glycero-3-phosphoethanolamine; $PIP_2$, phosphatidylinositol 4,5-bisphosphate; PC, phosphocholine; RMSD, root-mean-square deviation; MD, molecular dynamics; $SASA_{rel}$, relative solvent-accessible solvent areas; PHβ2, pleckstrin homology domain of PLCβ2; PLCβ2 chimera, PHβ2-PLCδ1 chimera; CPM, 7-diethylamino-3-(4′-maleimidylphenyl)-4-methylcoumarin; AS, anthryloxystearic acid; FRET, Förster resonance energy transfer; NBD, nitrobenzofurazanylamino dodecanoic acid; DOPC, dioleoyl phosphatidylcholine; DOPE, dioleoyl phosphatidylethanolamine;; LUV, large unilamellar vesicle; DABCYL, 4,4-dimethylamino-azobenzene-4′-carboxylic acid; $IP_3$, inositol trisphosphate.

enzyme can be further activated by Gβγ subunits (Jezyk et al., 2006; Hicks et al., 2008). It is noteworthy that the activation by Gβγ subunits is also conferred through the PH domain, as demonstrated by experiments in which the PH domain of PLCβ2 was swapped for that of PLCδ1 [which is not activated by Gβγ subunits (Wang et al., 2000)]. This exchange of activators was possible because of the high sequence conservation of the catalytic sites of the two enzymes. Further studies showed that enzymatic activity, membrane binding, and Gβγ activation of a PHβ2PLCδ1 chimera (referred to throughout as the "PLCβ2 chimera") were identical to those of full-length PLCβ2 (Wang et al., 2000; Drin et al., 2006). Because both Rac1 and Gβγ bind to membranes, and their activation of PLCβ2 is mediated by the PH domain, activation was suggested to involve recruitment of the PH domain to membranes (Hicks et al., 2008). However, PLCβ2 independently binds to membranes before Gβγ activation (Runnels et al., 1996), and cell studies show that PLCβ2 has a significant plasma membrane population (Guo et al., 2010). Because activation of PLCβ2 can also be achieved by a peptide derived from Gβγ (Gβ86–105) that does not interact with membranes (Buck et al., 1999), it is likely that activation by Gβγ is more complex, and rearrangement of the PLC protein domains relative to each other and to the membrane (Runnels et al., 1996; Drin et al., 2006).

Unlike PLCδ1, which binds to membranes that contain $PIP_2$ molecules via its PH domain (Rebecchi et al., 1992), membrane association of PLCβ2 shows little dependence on the nature of the lipid head group (Wang et al., 1999). Interchanging the PH domains of PLCβ2 and PLCδ1 was shown to lead to an exchange of their membrane binding specificities, demonstrating that binding of these enzymes to lipid membranes is determined by their PH domains (Wang et al., 2000), but the details of the PLCβ2 PH domain interaction with lipid membranes are unknown. It is noteworthy that activation of the PLCβ2 chimera by Gβγ or by Gβ86–105 is low when substrate is embedded in POPC bilayers and greatly enhanced in the presence of POPE (Drin et al., 2006). Thus, the nature of the membrane surface plays a key role in Gβγ activation of PLCβ2, but not binding.

To decipher the molecular details of PLCβ2 activation, we carried out molecular modeling of the interactions between the PH domain and 1) its own catalytic core, 2) one of its protein activators (Gβγ), and 3) phospholipid membranes and supported these findings experimentally. We identified the quaternary structures of an "active" PLCβ2 bound to Gβγ, and of PLCβ2 in a novel "inactive" conformational state using computational docking algorithms to predict protein-protein interactions that were substantiated by mutagenesis and spectroscopic measurements. Together, the results from our multiscale analysis yield a mechanistic model of the way in which PLCβ2 activity depends on protein-protein and protein-lipid interactions that occur at various time and length scales. A proposed mechanism of PH domain regulation of the PLCβ2 enzyme emerges from these results, in which the orientation of the PH domain with respect to the membrane surface plays a determinant role.

## Materials and Methods

**Protein-Protein Docking Algorithm.** A two-step docking procedure was used to predict the conformation of protein quaternary complexes. In the first step, termed "global search," a prepared ensemble of conformations of protein complexes is ranked with an energy-scoring function using two protein-protein docking software programs, ZDOCK (Chen et al., 2003) and PatchDock (Schneidman-Duhovny et al., 2003). These programs aim to search through the entire conformational space and rank the structures according to a calculated energy value (energy scoring function). Both have been shown to perform well in blind protein–protein docking competitions (Méndez et al., 2005), and the use of two different energy-scoring functions improves the chance of finding a true positive by reducing the bias that any one program might have. The programs were applied with the default parameters, and the top 2000 predictions from each were retained. The predictions from both programs were clustered based on RMSD. Representative structures from the largest clusters were designated as the most likely candidates for native protein-protein interaction complexes. The goal of this search is to retain at least one native-like conformation from among the top hits.

In the next step, termed the "local binding energy landscape calculation," the binding energy landscape of a given protein complex is tested to determine whether it is a local energy minimum. This was achieved by carrying out a Monte Carlo minimization scheme (known as a perturbation or refinement run) with the docking program RosettaDock (Gray et al., 2003). In this scheme, the complex is separated into two regions, a fixed "receptor" and a moveable "ligand." Starting from an initial prediction, a perturbation is applied to the position of the ligand: up to a 10-Å translation along a direction parallel to a line connecting the center of masses of the receptor and ligand, up to a 5-Å translation in the plane perpendicular to the same line, and up to a 10° rotation. The exact magnitude of these perturbations did not seem to affect the results. After the perturbation, the ligand is docked onto the receptor using a Monte Carlo minimization scheme with simultaneous side-chain optimization (Gray et al., 2003). The protocol was repeated 1000 times for each predicted complex solution, to generate a plot of RMSD with respect to the initial structure, versus the binding energy score. For a likely native structure, the points with the most negative binding energy score cluster in a shape indicative of a binding energy funnel. This method of identifying native protein-protein complexes by examining the shapes of binding energy landscapes has proven to be effective (London and Schueler-Furman, 2008).

**Coarse-Grained Molecular Dynamics Simulations.** Molecular dynamics simulations of the solvated lipid bilayer systems were performed using GROMACS version 3.3.1 (Van Der Spoel et al., 2005) and the coarse-grained MARTINI forcefield (Marrink et al., 2007). The bilayer system was simulated at 300 K using the Berendsen thermostat. The pressure was separately coupled in the membrane lateral and normal directions with Berendsen barostats set to 1 bar. The timestep used in these coarse-grained MD simulations was 40 ps.

For this simulation, a coarse-grained representation of the PLCβ2 PH domain was prepared from the all-atom coordinates of the crystal structure (Jezyk et al., 2006). The position of the backbone bead was the center of mass of the backbone of each residue. The coordinates of side-chain beads were also placed at the center of mass of the corresponding atoms taken from the same Protein Data Bank file. In the crystal structure, the 10 most N-terminal residues were not resolved. Therefore, they were first modeled in an extended conformation at the all-atom level before a coarse-grained model was constructed. In addition to the interactions specified in the MARTINI forcefield, harmonic restraints were also added between backbones beads in the protein that were less than 7 Å apart. This ensured that the overall tertiary structure available in the crystal was maintained throughout the simulation. These additional constraints were not added to the 10 most N-terminal residues, which were unresolved in the Protein Data Bank file (Jezyk et al., 2006).

**Relative Solvent-Accessible Solvent Areas.** $SASA_{rel}$ were measured using the program NACCESS (http://www.bioinf.manchester.

ac.uk/naccess/) with a probe radius of 1.4 Å and other default parameters.

**Protein Expression and Purification.** All PLC domain constructs, including the $His_6$-PLC$\delta$1, $His_6$-PLC$\beta$2 chimera, $His_6$-PLC$\beta$2 chimera mutants, $His_6$-PH domains, and the His6-catalytic domains were expressed in BL21D3 *Escherichia coli* and purified as described previously (Drin et al., 2006). Point mutants, the N-terminal deletion mutant of PH$\beta$2, and a single Cys construct in which all Cys residues except for Cys599 of the PLC$\beta\gamma$1 catalytic domain (11 total) were mutated to Ser using QuikChange (QIAGEN, Valencia, CA) also used this same expression and purification scheme. $G\beta_1\gamma_2$ subunits were prepared by coexpression of $G\alpha_q$, $G\beta_1$, and His6-$G\gamma_2$ in *Sf*9 cells and purified on a nickel-nitrilotriacetic acid column (Kozasa and Gilman, 1995). The purity of proteins was assessed by SDS-polyacrylamide gel electrophoresis gel and concentrations were determined by a Bradford assay (Bio-Rad) or by SDS-polyacrylamide gel electrophoresis with known concentrations of bovine serum albumin for reference. All PLC$\beta$2 constructs had activities near that (within 30%) of the wild-type full-length enzyme. The PLC$\beta$2 catalytic peptide 348–359 ($NH_2$-CFLEAIEAIESF-$CONH_2$) was purchased from the American Peptide Company (Sunnyvale, CA) with a purity >90% as confirmed by analytical high-performance liquid chromatography and mass spectrometry.

**Lipids.** POPE, POPC, palmitoyl-oleoyl phosphatidylserine, and $PIP_2$ in chloroform were purchased from Avanti Polar Lipids, Inc. (Alabaster, AL). [$^3$H]$PIP_2$ was from PerkinElmer Life and Analytical Sciences (Waltham, MA).

**Enzyme Activity Studies.** Measurements of $PIP_2$ hydrolysis by PLC enzymes were carried out using small, unilamellar vesicles composed of POPE/palmitoyl-oleoyl phosphatidylserine/$PIP_2$ at a 66:32:2 molar ratio doped with [$^3$H]$PIP_2$ (Drin et al., 2006).

**Fluorescence Labeling and Measurements.** Proteins were labeled on ice with the thiol-reactive probe 7-diethylamino-3-(4′-maleimidylphenyl)-4-methylcoumarin (CPM; Invitrogen, Carlsbad, CA) at a probe/protein ratio of 4:1. This same ratio was used in the time-course study (Fig. 12), except that the latter study was carried out at room temperature. The reaction was stopped after 60 min by adding 10 mM $\beta$-mercaptoethanol, and the protein was purified either by extensive dialysis or using a PD6 column (GE Healthcare; Chalfont St. Giles, Buckinghamshire, UK). PH$\beta$2 was also labeled on the N terminus with Alexa Fluor 488 2,4,6-trinitrophenol (Invitrogen) by raising the pH of the protein solution to 8.0 and incubating the probe with the protein for 1 h. The reaction was quenched by the addition of hydroxylamine and the labeled protein was isolated from unreacted probe using a 1-ml PD6 column followed by elution with 1 ml of 20 mM HEPES, pH 7.4, 150 mM NaCl, and 1 mM dithiothreitol buffer.

Fluorescence measurements were performed on a spectrofluorometer (ISS Inc., Champaign, IL) using 3-mm quartz cuvettes. Peptide and protein stocks were diluted into 20 mM HEPES, pH 7.2, 160 mM NaCl, and 1 mM dithiothreitol. Intrinsic fluorescence was monitored at $\lambda ex$ = 280 nm and scanning from 290 to 400 nm. The emission spectrum of CPM-labeled protein was measured from 415 to 630 nm ($\lambda ex$ = 384 nm). The background spectra of unlabeled protein or peptide were subtracted from each spectrum along the titration curve. All of the spectra were corrected for the 10 to 12% dilution that occurred during the titration. For the CPM time course study, the intensity was taken every 1 s at a single emission wavelength (560 nm).

FRET measurements to assess the orientation of Alexa Fluor 488-PH$\beta\gamma$2 on POPC versus POPC/POPE bilayers or of the CPM-labeled single Cys PLC$\beta$2 chimera was carried out by doping the bilayers with 0.5 mol % 6-anthryloxystearic acid (6-AS) or 12-AS or with 0.5 mol% NBD by adding the fatty acids from a concentrated solution in ethanol directly to preformed large unilamellar vesicles (LUVs) and sonicating the mixture for 10 min at low power in a bath sonicator. The relative FRET from AS donors to Alexa Fluor 488 was assessed by measuring the increase in Alexa emission exciting at 488 nm versus 381 nm, and the relative FRET from CPM donors to NBD was assessed by comparing the NBD emission exciting at 360 nm versus 480 nm. FRET efficiency was calculated by $E = (I - F_i(d - a)/F_i(d))$ where $F_i(d - a)$ is the fluorescence intensity of the donor in the presence of acceptor and $F_i(d)$ is the intensity for the donor alone.

**Membrane Binding Studies.** Membrane binding was carried out either by titrating LUVs (prepared by manual extrusion through 0.1 $\mu$m polycarbonate filter) into a 100 nM solution of labeled protein and by measuring the change in the integrated area of the probe spectra after correcting for background and dilution using the settings described above. Membrane binding of PH$\beta$2 and $\Delta N_{10}$-PH$\beta$2 was determined for both the His-tagged and cleaved protein. In these studies, LUVs were labeled with 0.1% Laurdan (Scarlata, 2002), and the emission was scanned from 400 to 580 nm with $\lambda ex$ = 360 nm. After correction for dilution and background, the change in fluorescence intensity was plotted as a function of lipid concentration and fit to a hyperbolic curve using SigmaPlot (Systat Software, Inc., San Jose, CA) to obtain the apparent partition coefficient ($K_p$), which corresponds to the lipid concentration at which 50% of the protein or peptide is bound.

## Results

**PLC$\beta$2-G$\beta\gamma$ Complex.** To derive a structural context for the activation of PLC$\beta$2 by G$\beta\gamma$, we used the crystal structure of a truncated form of PLC$\beta$2 (Jezyk et al., 2006) referred to throughout as PLC$\beta$2, for short) and the crystal structure of G$\beta\gamma$ (Lodowski et al., 2003) to perform an interaction energy-driven global search of the protein-protein docking space (see *Materials and Methods*). A set of candidate complexes containing the G$\beta\gamma$ heterodimer and PH, EF hand, CAT, and C2 domains of PLC$\beta$2, was obtained from this search using two different protein-protein docking programs, ZDOCK (Chen et al., 2003) and PatchDock (Schneidman-Duhovny et al., 2003). These candidates were then clustered based on RMSD, and representative structures from the largest clusters were retained for further analysis. Candidate complexes in which the G$\beta\gamma$ occluded the catalytic site of the CAT domain were removed, because this would be incompatible with activation. Likewise, we discarded any complexes in which the Rac1 binding site on PLC$\beta$2 was occluded by G$\beta\gamma$, because the G$\beta\gamma$ and Rac1 interaction surfaces are considered to be distinct (Jezyk et al., 2006). A representative structure from the largest cluster that met the above criteria (Fig. 1) was retained as a possible interaction complex.

To evaluate whether candidate complexes had native-like characteristics (for a discussion, see Shan et al., 2010), we constructed a local binding energy landscape for them and applied the criteria for identifying native-like structure, as described under *Materials and Methods*. In brief, RosettaDock (Gray et al., 2003) was used to apply a Monte Carlo minimization scheme to each starting complex. The resulting binding energies are plotted against the RMSD relative to the initial state. The local binding energy landscapes are shown in Fig. 2 for two different sets of protein complex ensembles. These binding energy landscapes were obtained by allowing either the G$\beta\gamma$ to move relative to a fixed PLC construct composed of the PH and CAT domains (Fig. 2, left), or the PH domain was moved relative to a fixed G$\beta\gamma$-PLC$\beta$2 catalytic core complex (Fig. 2, right). The initial orientation of the PH and CAT domain were taken from the crystal structures (Jezyk et al., 2006). The binding energy landscapes for both protein ensembles display the canonical funnel shape that is characteristic of native complexes (Gray et al., 2003).

To set up the experimental validation of the computationally derived model of the Gβγ-PLCβ2 complex, we identified positions in the PH domain that, according to the model, could directly affect the binding of Gβγ (and hence activation) upon mutation. A manually curated multiple sequence alignment of the PLCβ proteins and PLCδ1, shown in Fig. 3, was used to examine the amino acid identities in the interface with Gβγ in our model. Three contacts in the PLCβ2 PH domain, Lys71, Pro90, and Asp91, are conserved in PLCβ3, which is fully activated by Gβγ and where Lys71 is substituted by another basic residue, Arg. In contrast, these three residues are not conserved in PLCβ1 or PLCβ4, which are not activated by Gβγ subunits. There is some conservation of these residues in PLCδ1 (i.e., His for Lys71 and Glu for Asp91), which binds to Gβγ subunits with a weaker affinity than PLCβ2 but is not activated by these subunits. This lack of activation may also result from several deletions in this region (Fig. 3). In general, the pattern of conservation correlates well with the level of Gβγ binding and activation of these enzymes (Lee et al., 1994; Rebecchi and Scarlata, 1998; Wang et al., 1999).

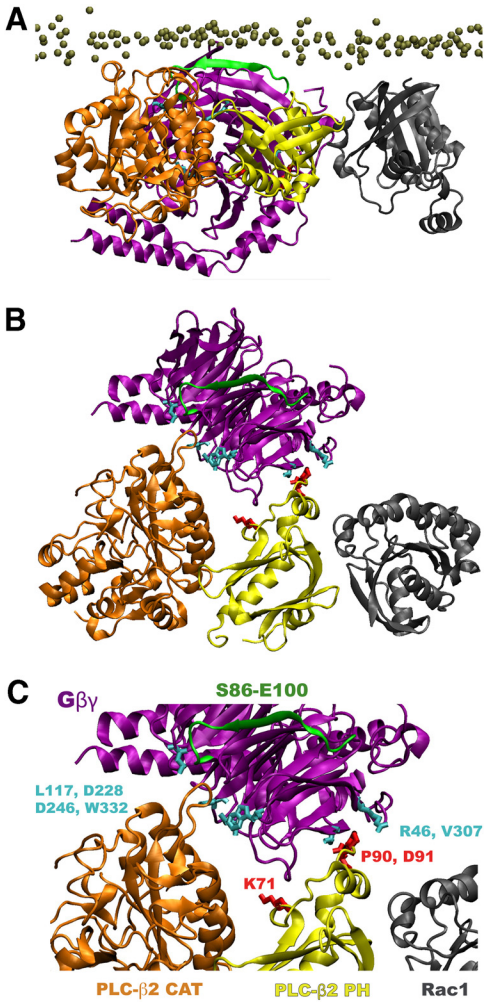


**Fig. 1.** Gβγ/truncated PLC-β2/Rac1"activated" complex. The PLC-β2 CAT domain is in orange, the PLC-β2 PH domain is in yellow, and Rac1is in gray. The arrangement of these three domains is taken from the crystal structure (Jezyk et al., 2006; Hicks et al., 2008). Gβγ is in purple, and its position represents the prediction from this work. A, side view, parallel to the membrane that is represented as yellow dots above the proteins. B, top view, same image as A, but rotated 90° to yield a view looking down from the membrane, in a perpendicular direction. C, Gβγ/truncated-PLC-β2 interactions highlighted in a close-up view, rotated 15° relative to B. Gβγ residues that make up the protein interface and are known to be involved in activation of PLC enzymes are shown in cyan (Arg46, Leu117, Asp228, Asp246, Val307, Trp332), and the stretch of residues 86 to 100, corresponding to the peptide that can independently activate PLC-β2, is highlighted in green. PLC-β2 residues that when mutated led to reduced Gβγ activation are shown in red (Lys71, Pro90, Asp91).

**Experimental Testing of the Structural Model of the PLCβ2-Gβγ Complex.** Studies were carried out using the PLCβ2 chimera, which has the highly conserved PLCδ1 catalytic core and lacks the C-terminal tail that has been implicated in dimerization of the enzyme (Wang et al., 2000; Ilkaeva et al., 2002) and is closely matched to the crystallographic structure that was used for our models. This PLCβ2 chimera construct is more readily manipulated because of successful bacterial expression, whereas its membrane binding, catalytic activity, and Gβγ activation properties are identical to those of full-length PLCβ2.

Two mutant enzymes were made. The first one had two mutations in the predicted Gβγ interface (Pro90, Asp91), whereas the second had mutations in all three Gβγ interface residues (Lys71, Pro90, Asp91). Because these residues are on surface sites, mutating these sites did not affect the basal activity of the enzyme. We tested the ability of these proteins to be activated by Gβγ subunits using a fluorescence-based assay. We found that even though the P90I/D91G double mutant still bound Gβγ, its level of activation was only ~15% of that seen for the wild type enzyme. In contrast, the K71A/P90I/D91G triple mutant no longer bound to Gβγ subunits and is no longer activated (Fig. 4, A and B). As a positive control, we measured the ability of the mutant to be activated by Gβ86–105, which has been shown to activate PLCβ2, PLCδ1, and the PHβ2 chimera (Buck et al., 1999; Drin et al., 2006), presumably through direct interactions with the catalytic domain. We find that the mutant was activated to the same extent as the nonmutated protein (Fig. 4C), demonstrating that the mutant maintained the ability to be activated. These results support the PHβ2-Gβγ interaction interface in the model shown in Fig. 1C.

**Inactive PLCβ2 Conformation.** To generate alternative models of PLCβ2 complexes that might represent inactive states, we searched for alternative docking positions of the PH domain to the EF-CAT-C2 components in the crystal structure of PLCβ2 (Jezyk et al., 2006). The PH domain was re-docked to a fixed EF-CAT-C2 domain scaffold using the Monte Carlo minimization scheme in RosettaDock (Gray et

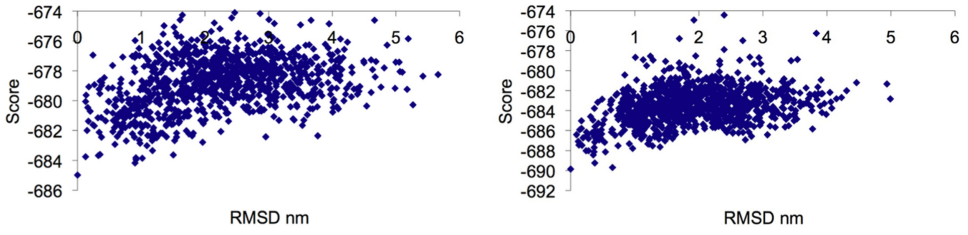


**Fig. 2.** Binding energy landscapes of PLCβ2 and Gβγ proteins. Left, Gβγ is treated as the moveable "ligand" and the PLC PH and CAT domains are treated as the fixed "receptor." Right, the PLC-PH domain is treated as the moveable "ligand" and the PLC-CAT and Gβγ proteins are treated as one fixed "receptor."

```
PLC        SHEETβ5 HX/TURN HELIXα2  LOOP HELIX SHEETβ6
β2_hum:  64 IRDTRFGKFAKMPKSQKLRDVFNMDFPDNSFLLKTLTVV 102
β2_rat:  64 IRDTRFGKFAKIPKSQKLREVFNMDFPDNHFLLKTFTVV 102
β4_rat:  65 INSIRLAAIPKDPKILAALESVGKSENDLEGR--ILCVC 101
δ1_rat:  72 IQEVRMGHRT-----EGLEKFA-RDIPEDR----CFSIV 100
β3_mus:  69 IRDTRTGRYARLPKDPKIREVLGFGGPDTRLEEKLMTVV 107
β1_bov:  69 VKDARCGKHAKAPKDPKLRELLDVGNIGRLEHR-MITVV 106
```

**Fig. 3.** Sequence analysis of PLC-$\beta$ proteins in the region of the PH domain that interacts with G$\beta\gamma$. The highlighted residues show the residues (Lys71, Pro90, Asp91) in the human PH$\beta$ that contact G$\beta\gamma$ in our model. The SS (secondary structure) corresponds to the known PH$\beta$2 structure (Jezyk et al., 2006; Hicks et al., 2008). We manually obtained this alignment by 1) aligning $\beta$5 and $\beta$6, 2) aligning helix$\alpha$2, and then 3) aligning the intervening regions as best as we could.

al., 2003) as described under *Materials and Methods*. We note that for this procedure, the linker between the PH and EF domains (residues Leu138–Asn141) was removed, but the final models were checked for the ability to accommodate the linker and accepted only if the condition was met. Figure 5A shows that the resulting RMSD versus energy score plot displayed a binding energy funnel, in accordance with the criterion for a native binding site for the original configuration taken from the crystal structure (see Fig. 6, A and C for the relative positions of the PH and CAT domain in this complex). Also in Fig. 5, left, there is an additional configuration, located 15 Å from the original (marked by the arrow), which has the same excellent score. Performing the same computational probing of the energy pattern around this structure (carried out as for the crystal structure and found to resemble a canonical binding energy funnel as shown in Fig. 5, right) indicates that the this configuration indeed represents a native binding mode.

**Experimental Support for an "Inactive" PLC$\beta$2 Structural Model.** We tested the validity of alternative model found as described above and shown in Fig. 6. Because the interface between the PH and catalytic domains in this complex is distinct from that in the crystal structure, we focused on this region. We first verified the relation between this interface and the other complexes by evaluating the $SASA_{rel}$ for a sequence of residues in this interface (i.e., 384–396 of the PLC$\beta$2-CAT domain) in the isolated CAT-EF2-C2 domains and in the PH–CAT-EF2-C2 complex in both the active and "inactive" conformations (see Table 1). Defining residues with $SASA_{rel} > 15\%$ as "solvent exposed" (as opposed to "buried"), we found that only six residues (Table 1, bold) were solvent-accessible in both the "active" and "inactive" CAT-EF2-C2 domains. It is noteworthy that four of these become "buried" in the "inactive" PH–CAT-EF2-C2, whereas none is changed in the "active" structure of the complex compared with the isolated domain. This result indicates that residues 384 to 396 are part of an interface between the PH and CAT domain in the "inactive" conformation, but not in the active one.

We tested the predicted PH-CAT interface (Fig. 6) by synthesizing a peptide corresponding to residues 384 to 396 of the catalytic domain and experimentally determining its ability to disrupt interactions between the PH and catalytic domains. These studies were carried out measuring the binding of isolated PH$\beta$2 and PH$\delta$1 to the catalytic core in the absence or presence of this peptide. In the absence of peptide, the PH$\beta$2 and PH$\delta$1 bound to the catalytic domain, but this observed binding was eliminated in the presence of peptide (Fig. 7A). This inhibition of PH-CAT binding by the peptide is considered to be due to the strong binding between the peptide and the PH domain, observed in solution (Fig. 7B). It is noteworthy that this peptide did not bind at all to the whole PLC$\delta$1 enzyme or its isolated catalytic domain, but it did interact weakly with the PLC-$\delta$1 PH domain.

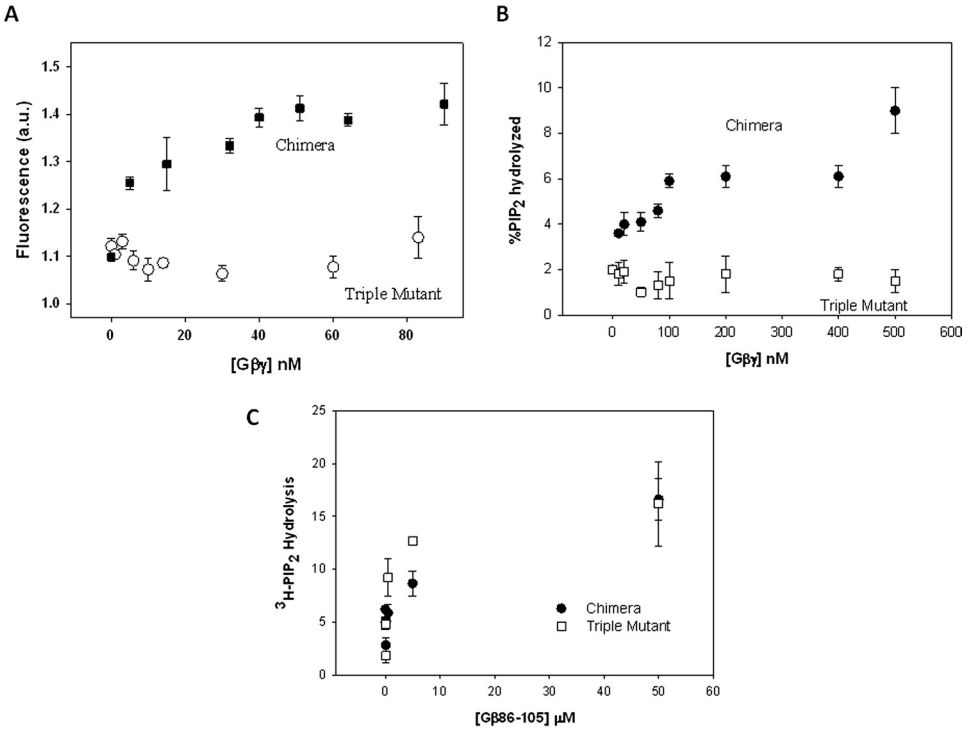


**Fig. 4.** Binding of G$\beta\gamma$ subunits with PLC proteins is disrupted by substitutions in the PH domain of PLC-$\beta$2. A, binding of purified G$\beta\gamma$ subunits to the CPM-labeled PLC$\beta$2 chimera wild type and the K71A/P90I/D91G triple mutant reconstituted on PC/phosphoserine/PE (1:1:1) lipid bilayers as G$\beta\gamma$ is incrementally added. Shown is the normalized integrated fluorescence intensity of the CPM protein ($n$ = 3 and S.D. is shown) as a function of G$\beta\gamma$ concentration. B and C, increase in enzymatic activity of PLC$\beta$2 chimera wild type and K71A/P90I/D91G triple mutant by G$\beta\gamma$ subunits (B) and by the peptide G$\beta$86–105 (C); $n$ = 3 and S.D. is shown.

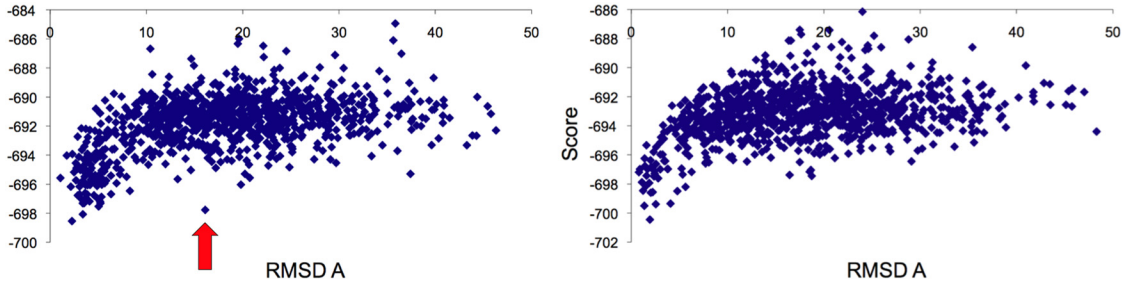


**Fig. 5.** Binding energy versus RMSD plot for the interaction between the PH domain and the EF-CAT-C2 catalytic core. Left, initial and reference conformation is taken from the crystal structure of a PLC-β2 construct. The red arrow points to a high scoring structure, shown in Fig. 6. Right, initial and reference conformation is taken from the docking output in the left panel, indicated by the red arrow.

The combined inferences from our computational and experimental findings lead us to propose that the PLCβ2 complex shown in Fig. 6, B and D, which is different from the one seen in the crystal structures (Jezyk et al., 2006; Hicks et al., 2008), is a native binding mode that represents the inactive conformation of PLCβ2. In further support of this proposition, we find that the interface contains residues Lys80 and Arg82 of the PH domain that were found in other experiments to stabilize the inactive complex (Drin et al., 2006).

**Membrane Binding Studies Support Alternate Models of PLCβ2.** Previous studies suggest that the orientation of the PH domain relative to the catalytic domain is altered upon membrane binding (Drin et al., 2006). Because the PLCβ2-PH domain also determines the binding affinity and specificity for phospholipid membranes (Wang et al., 1999), it is likely to be important for regulation of PLC activity. However, the arrangement of domains as seen in the crystal structure (Jezyk et al., 2006; Hicks et al., 2008) and in the combined activated complex with Gβγ (Fig. 1A) does not seem to allow for direct membrane interaction of the PH domain despite the need for this domain to target the host enzyme to the membrane surface. We reasoned that another conformational state exists, such as the one presented in Fig. 6, in which PLCβ2 interacts with membranes directly through its PH domain. To this end, we sought to identify the surface of the PH domain that interacts with lipid membranes. These studies were carried out through MD simulations with a coarse-grained model of a solvated lipid bilayer and a PLCβ2 PH domain comprising residues 1 to 144 (see *Materials and Methods* for details).

The coarse-grained model of the PLCβ2 PH domain was initially placed outside of a mixed lipid membrane system (see Fig. 8A) that contained 341 DOPC and 170 DOPE lipids (~2:1). The simulation system contained ~$1.5 \times 10^4$ water beads, which provides ample volume for the PH domain to diffuse freely. During the MD simulations, the protein diffused in the solution without associating with the membrane until $t = 0.6$ μs; at this point, the N-terminal end of the PH domain began to interact with the interfacial region of the

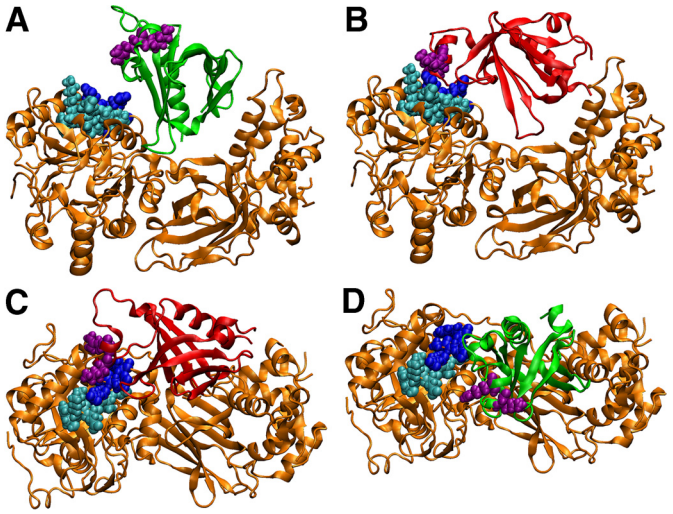


**Fig. 6.** Difference between the active and inactive states involves both a translation and a rotation of the PH domain (shown in green for the active complex and in red for the inactive complex), with respect to the CAT-EF2-C2 domain (shown in orange). Residues that were previously mutated and reported to decrease the basal level of signaling (Drin et al., 2006) are shown in purple van der Waals (VdW) representation (Lys80/Arg82 from the PH domain). Residues 384 to 396 of the CAT domain, which were used as a peptide template to test our modeled "inactive" complex conformation are shown in cyan VdW representation, except for residues 389, 392, 393, and 396, which interact with the PH domain and are shown in blue VdW representation. A and B, orthographic "side" view of the active complex taken from the crystal structure (A) and the inactive complex (B). C and D, orthographic "top" view of the active complex (from the crystal) (C) and the inactive complex (D).

TABLE 1

Relative SASA values (as measured with the program NACCESS (http://www.bioinf.manchester.ac.uk/naccess/) measured in the "active" crystal and "inactive" model for residues 384 to 396 for an isolated CAT-EF2-C2 domain and in the context of the PH–CAT-EF2-C2 complex. Defining a residue with $SASA_{rel} > 15\%$ as "exposed" and "buried" otherwise, one can observe six residues (marked in bold) in both the active and inactive AT-EF2-C2 domains, among which four become "buried" in the "inactive" PH–CAT-EF2-C2, but none in the active one. Shown are $SASA_{rel}$ values of residues Phe384 to Phe396 in the CAT-EF2-C2 domain in isolation ("CAT-EF2-C2") and in complex with the PH domain ("PH–CAT-EF2-C2"), respectively, for both the active and inactive conformations. Highlighted in bold are the residues that undergo significant decreases in $SASA_{rel}$ because of contact with the PH domain, undergo a significant decreases in $SASA_{rel}$.

| CAT Residue | $SASA_{rel}$ | | | |
|---|---|---|---|---|
| | Active | | Inactive | |
| | PH–CAT-EF2-C2 | CAT-EF2-C2 | PH–CAT-EF2-C2 | CAT-EF2-C2 |
| | % | | | |
| Phe384 | 0.1 | 0 | 0 | 0 |
| Lys385 | 41.1 | 59.9 | 47.9 | 59.9 |
| Glu386 | 41.3 | 40.9 | 41.8 | 41.8 |
| Ala387 | 0 | 0 | 0 | 0 |
| Ile388 | 0 | 0 | 0 | 0 |
| **Glu389** | **43.3** | **36.9** | **15.4** | **41.7** |
| Ala390 | 0 | 0 | 1.2 | 11.2 |
| Ile391 | 0 | 0 | 0 | 0 |
| **Ala392** | **19.5** | **20** | **0** | **21.2** |
| **Glu393** | **18.8** | **46.1** | **0** | **65.8** |
| Ser394 | 1.4 | 0 | 0 | 0 |
| Ala395 | 0 | 0.5 | 0 | 0.5 |
| **Phe396** | **24.8** | **23.5** | **2.8** | **24.8** |

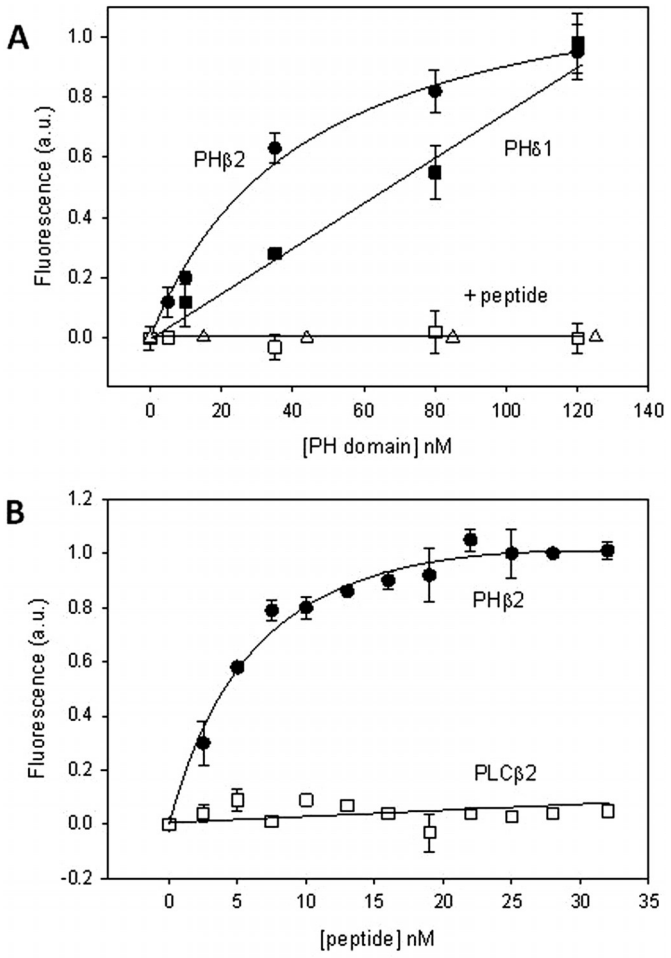


**Fig. 7.** Peptide inhibition of PH-CAT binding supports inactive model. A, binding of the PH domains of PLC$\beta$2 and PLC$\delta$1 to the CAT domain of PLC$\delta$1 labeled with CPM where binding is seen as an increase in CPM fluorescence. No changes in fluorescence of CPM-CAT are observed in the presence of 600 nM the peptide PLC$\beta$2(385–394), which is a segment corresponding to a region that lies in the interface of the inactive state model, when either PH$\beta$2 or PH$\delta$1 are added (note that an offset of +5 was added to the $x$ value of these data to allow them to be seen). All data are an average of three trials, and S.D. is shown. B, binding of the PLC$\beta$2 (385–394) peptide to CM-PH$\beta$2 in solution (●) or to CM-PLC$\beta$2 (○); $n$ = 3 and S.D. is shown.

membrane (see Fig. 8B). Soon thereafter, several other residues from the N-terminal end of the protein, up to residue 10, were found to lie on the surface of the phospholipid bilayer and remained that way for the duration of the simulation (see Fig. 8C). A parallel simulation with the same lipid membrane system, but with a PLC$\beta$2 PH domain where the first 10 residues were deleted, was performed under identical conditions for 2 $\mu$s. This protein never achieved a sustained membrane association (data not shown).

These observations suggest that the N-terminal residues of the PH domain are necessary for its interaction with lipid membranes. We confirmed the impact of these residues on membrane binding experimentally by testing in vitro a PLC$\beta$2-PH domain in which the first 10 residues were deleted (see *Materials and Methods*). In agreement with our computational simulations, Fig. 9 shows that the membrane binding affinity of this truncated construct for both POPC and mixed POPC/POPE membranes is significantly lower than measured for the wild-type.

G$\beta\gamma$ activation of PLC$\beta$2 seems to be inhibited by PC lipids, but increasing the concentration of PE headgroups leads to full activation (Drin et al., 2006). We therefore hypothesized that there may be differences in the nature of the interaction between PLC$\beta$2 PH domains and lipid membranes that also depend on the concentration of PE lipid headgroups, and that this might account for the differential response to G$\beta\gamma$. This hypothesis was tested computationally with a coarse-grained protein-bilayer interaction model of a PLC$\beta$2-PH domain binding with its N-terminal region to bilayers with a series of different DOPC/DOPE lipid ratios: all DOPC, 2:1 DOPC/DOPE, 1:1 DOPC/DOPE, and 1:2 DOPC/DOPE. The simulations were performed for solvated bilayer systems containing 200 total lipids and $\sim 3 \times 10^3$ water beads, and each system representing a different lipid ratio was simulated for 2.5 $\mu$s (see *Materials and Methods* for more details). In this set of simulations, only residues 1 to 135 of the PH domain were included, to eliminate a spurious interaction observed in the previous simulation, between the membrane and the C-terminal residue (144); in the full protein, this residue is connected to the EF domain and would not be available for membrane interaction.

The nature of the PH domain-membrane interaction was found to depend on membrane composition. Specifically, we found that the distance of residue Thr30 from the center of the bilayer strongly correlated with the PE lipid concentration. Thr30 was chosen as an indicator of PH domain orientation because it is positioned on the opposite surface from the N terminus. Thus changes to the orientation of the N-terminal-membrane bound PH domain are reflected in the distance between residue Thr30 and the membrane. Figure 10 shows that the Thr30-membrane distance, presented as the average value from the last half of the simulation, decreases as the concentration of DOPE increases. Two representative snapshots showing the orientation of the PH domain with Thr30

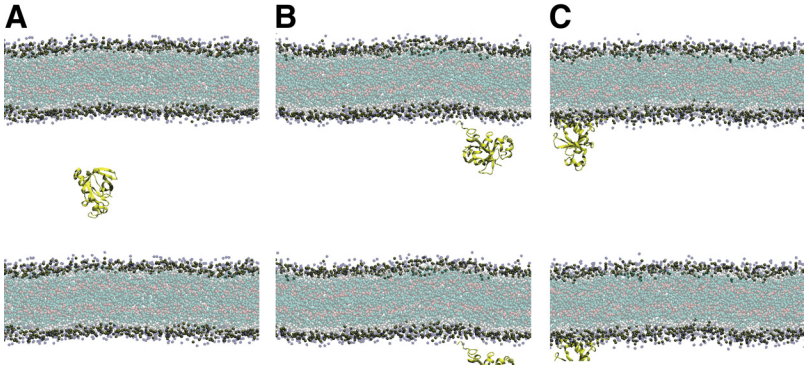


**Fig. 8.** Snapshots from the coarse-grained molecular dynamics simulation of the PLC$\beta$2 PH domain and a hydrated phospholipid membrane taken at $t$ = 0.5, 0.6 and 1.4 $\mu$s (A–C). The lipid membrane is shown above the protein as colored points, and the water was omitted for clarity. Note that these images include one periodic image in the vertical direction to illustrate the size of the box.

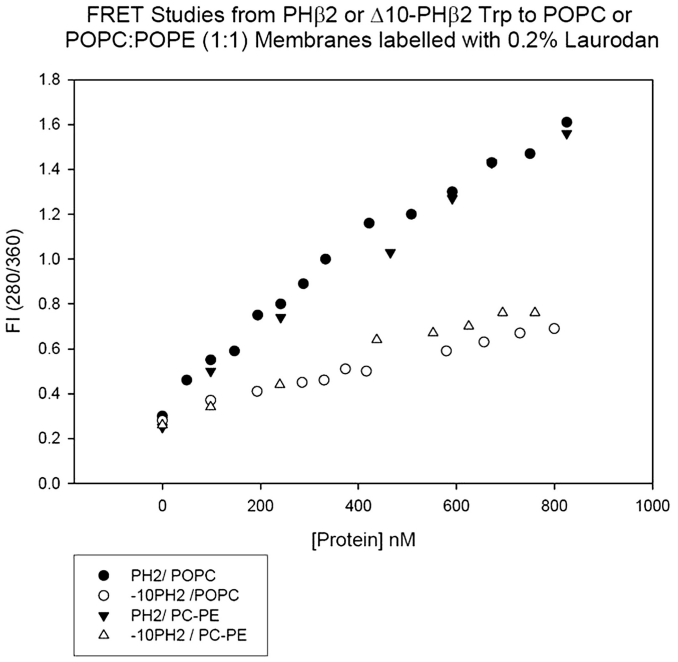


**Fig. 9.** Binding of PHβ2 and Δ10-PHβ2 to membranes composed of 100% POPC or POPC/POPE 1:1 doped with 0.2% Laurdan as measured by the amount of FRET from PH domain Trp residues to Laurdan. Relative FRET was assessed from increase in emission from the Laurdan acceptors when the Trp donors are excited (i.e., at 280 nm), compared with the intensity obtained when only Laurdan is excited at 360 nm. These data show that PHβ2 binds equally well to POPC and PC/PE bilayers (filled symbols) but that deletion of the first 10 N-terminal residues greatly diminishes binding to both types of membrane (open circles). All curves are an average of three trials, and the maximum error is ± 0.08.

far from the membrane and close to the membrane are shown in Fig. 11, A and B, respectively. In addition, when the CAT domain was placed beside the PH domain as in the proposed inactive state (Fig. 6B), the conformation favored in the membranes enriched with DOPE, positions the CAT domain closer to the membrane (Fig. 11B) and thus in better position for activation by a membrane-bound Gβγ.

We found through experimentation that differences in the nature of PH domain association to membranes determined in the presence of PE headgroups were also detectable in FRET studies. In general, the degree of FRET is sensitive to the distance between the fluorophores. We labeled the N terminus of PHβ2 with a FRET acceptor, Alexa Fluor 488, and measured the ability of two FRET donors, 6-AS and 12-AS, to transfer energy to the Alexa Fluor 488-labeled protein. For freely rotating probes, the distance at which 50% FRET occurs (i.e., the $R_o$) for this pair is ~20 Å. Because we do not expect the membrane-localized probes to be freely rotating, we used FRET as an indicator of differences in the distance/orientation of the N terminus of the protein in POPC versus POPC/POPE 1:2 membranes. We found that the FRET efficiency (0.57 ± 0.04) from Alexa Fluor 488-PHβ2 to the more shallow probe 6AS, was identical in POPC and POPC/POPE 1:2 bilayers. These results suggest a similar distance and orientation of the N terminus of PHβ2 to 6-AS in both membrane types. In contrast, significant differences in FRET were observed for 12-AS, the FRET efficiency being less in POPC (0.27 ± 0.01) bilayers than in POPC/POPE (0.40 ± 0.01) bilayers. These results suggest that the N terminus of PHβ2 is either more deeply buried when PE is

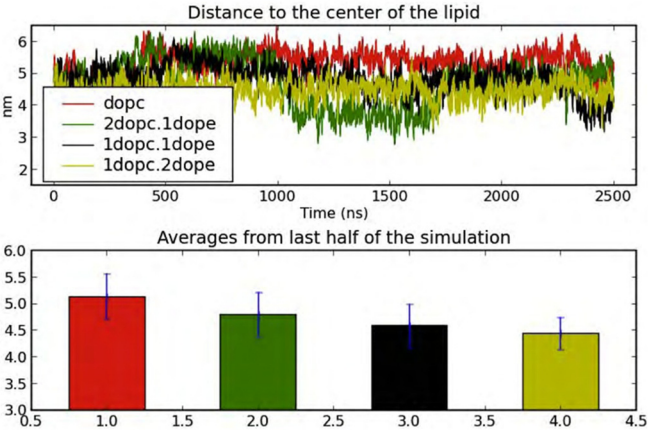


**Fig. 10.** Position of Thr30 relative to the center of the lipid bilayer in coarse-grained MD simulations.

present or is in a better orientation to allow for FRET with the 12-AS probe. In either case, these measurements show that the interaction of the N terminus of PHβ2 with membranes differs in the presence and absence of POPE.

**Experimental Testing of PLCβ2 Conformational Changes on PC- versus PE-Containing Membranes.** Our studies suggest a model in which PLCβ2 binds to PC bilayers by insertion of its first 10 residues that causes its catalytic domain to be far from the membrane surface and

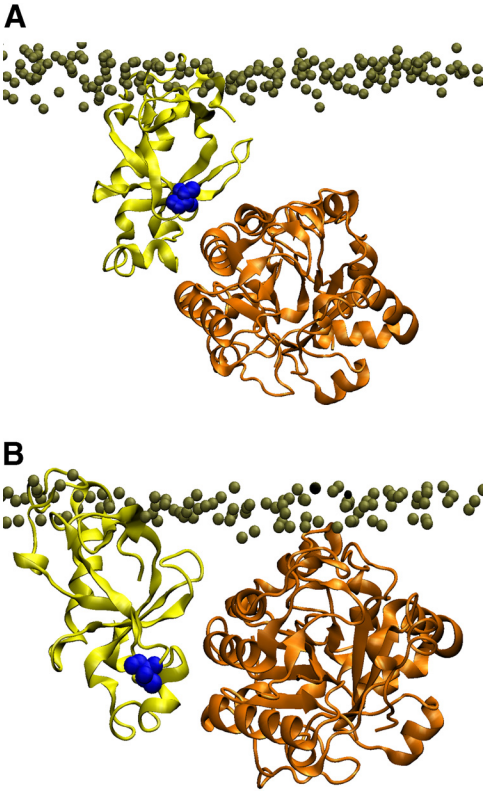


**Fig. 11.** Sample of extreme PH domain orientations observed during the coarse-grained molecular dynamics simulations. The PH domain is rendered in yellow, with residue Thr30 (in blue) rendered in a van der Waals representation. The CAT domain is rendered in orange and placed relative to the PH domain as it is found in its predicted inactive state conformation from Fig. 6B. A, snapshot at $t$ = 480 ns, showing Thr30 far from the lipid membrane, which is favored in DOPE-depleted membranes. B, snapshot at $t$ = 1400 ns, showing Thr30 far from the lipid membrane, which is favored in DOPE-enriched membranes.

unable to be activated by G$\beta\gamma$ subunits. In contrast, the more nonpolar PE-containing membrane surface promotes different enzyme orientations in which the catalytic domain is close to the membrane surface and can contact G$\beta\gamma$ subunits.

We carried out a series of fluorescence-based studies to test this model. First, we determined differences in the reactivity of PLC$\beta$'s Cys residues when the protein is bound to pure POPC versus POPC/POPE 1:2 LUVs. CPM is not fluorescent in its unreacted form but becomes highly fluorescent when it covalently attaches to thiol groups. We monitored the increase in CPM fluorescence at 560 nm when it was added to a 100 nM solution of PLC$\beta$2 bound to 100 $\mu$M POPC or 100 $\mu$M POPC/POPE 1:2 membranes. A sample trace is shown in Fig. 12A. Although the time course varied slightly for each sample as a result of experimental error, the maximal value consistently showed a 3-fold higher intensity of CPM when the protein was bound to PE-containing membranes ($n$ = 4).

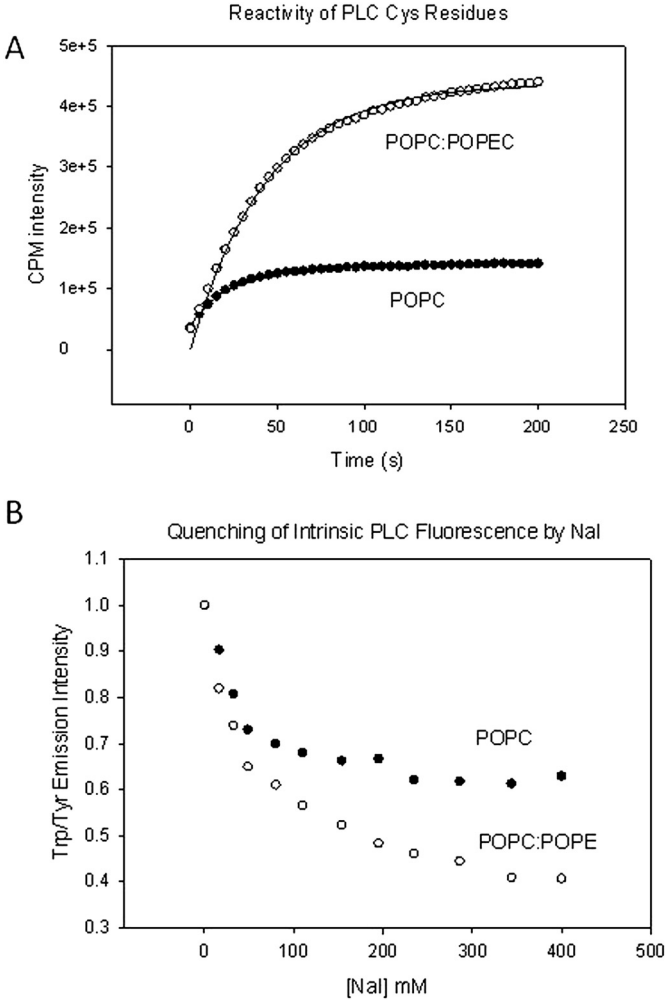


**Fig. 12.** A, time course of the increase of CPM fluorescence, as monitored at $\lambda$ex = 380 nm and $\lambda$em = 560 nm upon covalent attachment to PLC$\beta$2. In this study, 100 nM PLC$\beta$2 was prebound to either 100 $\mu$M POPC or 100 $\mu$M POPC/POPE 1:2 LUVs by simple addition. The reaction was initiated by the addition of 400 nM CPM to the cuvette at room temperature. Addition of CPM to membranes alone did not produce any change in fluorescence. B, comparison of the loss in intrinsic intensity of PLC$\beta$2 by Trp and Try side chains due to quenching by NaI bound to POPC or POPC/POPE 1:2 LUVs. Studies were carried out exciting the samples at 280 nm and monitoring the integrated intensity from 290 to 400 nm. Experimental error (not shown) was less than 2% and $n$ = 3.

This result is in accord with a larger number of orientations on PE-containing lipids being sampled by the enzyme.

The differences in protein-membrane orientations resulting from the presence of PE-containing lipids were monitored in an alternate series of studies measuring the solvent exposure of Trp/Tyr residues of PLC$\beta$2 bound to POPC versus POPC/POPE 1:2 LUVs. Trp and Tyr residues are responsible for the intrinsic fluorescence of PLC$\beta$2 and these residues are quenched by collision with iodide ions. Therefore, the degree of fluorescence quenching by iodide ions will indicate differences in the ability of $I^-$ in solution to contact the Trp/Tyr when bound to the two different types of lipid membranes. In Fig. 12B, we show that the degree of $I^-$ quenching is similar for both samples at low amounts of added NaI, suggesting that the most accessible residues are equally accessible with both lipid surfaces. However, at high NaI, the quenching curve shows that the Trp/Tyr residues of PLC$\beta$2 on PC membranes are far more protected from quencher compared with the PC/PE system. Because Tyr/Trp residues are spread throughout the protein, the higher degree of quenching on PE membrane is consistent with accessibility to a larger number of protein-membrane orientations on these surfaces, compared with PC membranes.

We then investigated whether the conformation promoted by the PE lipids positions the catalytic domain closer to the membrane surface. For these studies, we constructed a PLC$\beta$2 chimera containing a single Cys residue (Cys599) located in the catalytic domain. Using this mutant, we can determine the differences in the relative distance between the labeled site in the catalytic domain and a fluorescent probe on the membrane surface (NBD) by FRET measurements. FRET value of negative controls were measured in the absence of CPM donor molecules and positive controls consisting of doubly labeled NBD-bovine serum albumin-CPM, we find that when the enzyme is bound to PE membranes the amount of FRET is 37 $\pm$ 8% higher than on PC membranes. This result shows that PE lipids allow the catalytic domain of the enzyme to move close to the membrane surface (Fig. 11).

To test the prediction from our model that a different orientation is achieved between the PH and catalytic domains on PC membranes compared with PE-containing membranes, we used FRET to estimate the differences in the distance between Cys599 and the N terminus of the enzyme on the two types of membranes. In our molecular models, the distance is shorter in the active complex than in the PC-bound inactive model. To probe this prediction, we labeled the single Cys with CPM and placed a FRET acceptor on the N terminus (DABCYL). DABCYL is a nonfluorescent FRET acceptor and the $R_o$, or distance at which 50% CPM is transferred to DABCYL, is 22 Å (van der Meer, 1994). Keeping in mind that the enzyme has an N-terminal $His_6$ tag, we find that attachment of DABCYL to the N terminus results in a large decrease in CPM intensity giving a FRET efficiency of 62 $\pm$ 13%. Binding of the enzyme to PC membranes nearly eliminates FRET (efficiency is close to zero at 2 $\pm$ 8%). This loss in FRET is consistent with an increased distance between the N terminus and the catalytic domain as a result of its insertion into the bilayer. In contrast, binding to PE lipids increases the FRET efficiency to 83 $\pm$ 9, consistent with the large differences we find in our studies for the domain orientations in the two types of lipid compositions.

## Discussion

Because of the physiological significance of PLCβ2, the mechanisms determining its regulation have engendered great interest. Past work has identified protein activators of PLCβ2 on different membrane surfaces, but many of the molecular details regarding activation of the enzyme remain largely undetermined. To reveal essential elements of these mechanisms, we used a combination of correlated computational and experimental approaches to construct and interrogate molecular models of the active and inactive complexes. Starting from the configuration of PLCβ2 identified in the crystal structure of one molecular state (Jezyk et al., 2006; Hicks et al., 2008), we constructed a model of the PLCβ2/Gβγ complex without any conformational changes to the backbone of the PLCβ domains, which supports the notion that the configuration shown in the crystal structures represents an activated state. Our model of the PLCβ2/Gβγ complex agrees well with past experimental work. For example, several residues in Gβ (Arg46, Val307, Leu117, Trp332, Asp228, and Asp246) that were previously identified as being important for Gβγ mediated activation of PLCβ2 (Li et al., 1998; Panchenko et al., 1998) were found to make up part of this complex's interface (Fig. 1C). In addition, Gβ86–105, which has been shown to produce activation of both PLCβ2 and PLCδ1 (Buck et al., 1999; Drin et al., 2006), interacts directly with the catalytic domain in our model, as predicted from its ability to activate the isolated catalytic domain as well as the whole enzymes. Furthermore, our model accounts for the fact that activation by Gβγ is achieved for PLCβ2, but not the related PLCδ1, by identifying the interaction site on the PLCβ2-PH domain as a region of sequence not found in PLCδ1 (identifiable as an insert in the alignment; Fig. 3). To our knowledge, there is only one study that proposes another Gβγ binding site (Bonacci et al., 2005). This suggestion was based on triple alanine mutants in the catalytic domain. However, this catalytic site is highly conserved in PLCβ2 and PLCδ1, as well as in other PLCs that are not activated by Gβγ. In addition, mutations in this region affected catalytic activity as well as Gβγ activation, making it difficult to uncouple the possible effects arising from structural changes in the catalytic site, from those involving changes in Gβγ activation.

Given the arrangement of the PLC domains in the crystal structures (Jezyk et al., 2006; Hicks et al., 2008), it remained unclear how the PH domain could achieve the interaction with lipid membranes suggested from experimental evidence showing that the PH domain is the key mediator of lipid membrane association (Drin et al., 2006). We reasoned that there was likely to be at least one other conformational state of PLCβ2 in which the PH domain interacts with membranes, and we hypothesized that it would have features resembling the catalytically inactive state, because it precedes Gβγ binding and activation. Note that the two crystal structures of the system (Jezyk et al., 2006; Hicks et al., 2008), are very similar except for an anionic linker region that connects the two halves of the catalytic domain. Both structures show that in the absence of activator, the linker occludes the active site, and studies have shown that mutations and deletions of the linker region produce a more active enzyme that can still be activated by Gα, Gβγ, and Rac1 (Jezyk et al., 2006; Hicks et al., 2008).These authors had suggested that enzyme activation occurs through the displacement of this linker by the membrane surface. As discussed below, a great number of solution studies suggest that this relief of autoinhibitory interactions is not the only mechanism of PLCβ2 activation by Gβγ subunits and that different activation routes lead to different levels of activity. Therefore, given their great similarity of the crystal structures and the evidence for allosteric regulation, both structures were considered to represent the activated state.

We thus set out to determine inactive forms of the enzyme. Because the PH domain is required for membrane binding of the truncated enzyme, we used a combination of computational modeling and experimental validation to identify the orientation of a membrane-bound PH domain, which involves insertion of its N-terminal residues, and generated an alternative combined structure for the PH and CAT domains. It is noteworthy that the positioning of the new PH-CAT domain complex that allows the insertion of the N-terminal region of the PH domain into a lipid membrane prevents the CAT domain's catalytic site from facing the membrane (see Fig. 11). The inability of this complex to catalyze $PIP_2$ hydrolysis is further suggested by the configuration in which simultaneous interactions of the PH domain with both the lipid membrane and the catalytic domain, as we described, place the CAT domain in an orientation that prevents catalysis. As detailed below, the propensity to achieve reorientation depends on the nature of the lipid surface that the enzyme is bound. This suggestion correlates well with observation that Gβγ activation occurs on PE but not PC membranes (Drin et al., 2006) and with our computational studies showing that PE lipids allow for domain reorientation. We propose that to stimulate the enzyme, an additional interaction is required to stabilize the orientation of the PH domain relative to lipid membranes to produce a rearrangement within the CAT domain backbone and/or productive membrane orientation of the catalytic domain. This productive configuration of the membrane-bound PH-CAT domain is certainly expected to promote detachment of the anionic linker from the active site, which has been previously suggested from crystallographic studies (Hicks et al., 2008). This reorientation requires the binding of G protein activators, which have their own preferred orientation relative to the membrane surface, to reorient the PH domain and the attached CAT domain on the membrane surface. This reorientation promotes detachment of the anionic loop to open the active, as suggested previously (Jezyk et al., 2006; Hicks et al., 2008), and move the conformation of the enzyme from a structure based on the one presented in Fig. 11b to one seen in Fig. 1. The large change in FRET between sites in the catalytic and PH domains we report here supports this idea. The directed series of rearrangements we propose in our model as the result of specific interaction at alternate interfaces constitutes a mechanism that is somewhat different from the "scooting mechanism" of PLCδ1, in which binding of the PH domain to a $PIP_2$ lipid molecule alters the orientation between the PH and CAT domains to allow for activation without other external protein interactions.

We note that the structural difference we propose between the PLCβ2 PH domain in the crystal structures (active-like state) and the N-terminally membrane-bound domain (inactive-like state; see Fig. 11) involves a large rotation of at least 90°, making it seem as if G proteins must induce a large

change in PLC$\beta$2 orientation for activation. However, we found that although the PH domain always inserts its N-terminal residues into the interfacial region of membranes for binding, regardless of membrane composition, the orientation of the PH domain on membrane surfaces was quite variable depending on the concentration of PE headgroups. Specifically, the PH domain penetrated more deeply and sampled orientations that were more similar to the one seen in the active-like crystal state when it is was associated with membranes that contained PE lipids in a concentration-dependent manner. This implies that the change in the orientation from a PH-membrane bound inactive to an activated state may be reduced significantly depending on the membrane composition. Furthermore, membranes that contain PE headgroups may allow the PH domain and its associated CAT domain to preferentially sample states that are closer to the active-like state and can therefore more easily bind to G$\beta\gamma$. As noted, these differences in PH domain orientation that depend on the concentration of PE headgroups in the membrane may account for the increased potency of activation of PLC$\beta$2 (Drin et al., 2006). The PH domain serves a unique role in PLC$\beta$2 regulation. It plays an inhibitory role when it is bound to lipid membrane surfaces, yet it confers activation when it encounters G$\beta\gamma$ or Rac1. Although we began by identifying the molecular interactions that are essential to stabilize the various PH complexes, other key questions concerning the differential response of PLC$\beta$2 to G$\beta\gamma$ could only be answered when the dynamics on the PH domain on membrane surfaces were considered.

We acknowledge that the molecular mechanism of by which G$\beta\gamma$ binding moves the preactive conformation into the fully active one is not clear. It is possible that the initial binding allows for movement of the PH and CAT domains in a sequential manner, and it is also possible that the membrane orientation of G$\beta\gamma$ subunits differs in the free and PLC$\beta$2-bound states. Current studies to determine these movements are under way. Regardless of these uncertainties, it is tempting to propose that a possible mechanistic role for the reorientation of the CAT domain relative to the membrane after G$\beta\gamma$ binding helps the enzymatic reaction by facilitating product release. We have found that G$\beta\gamma$ activates the second half of the $PIP_2$ hydrolysis (Feng et al., 2005). This hydrolysis occurs in two steps: cleavage of the DAG from the head group to give a cyclic $IP_3$ and then hydrolysis to give the linear $IP_3$. It is noteworthy that in contrast to other PLCs, PLC$\beta$2 and the PH$\beta$2-PLC$\delta$1 chimera only produce linear $IP_3$ showing that the product of the first reaction is held in the active site long enough for water to attack the substrate (Feng et al., 2005). It is possible that binding of G$\beta\gamma$ helps to reorient the catalytic site from the membrane to allow for increased product release.

**Acknowledgments**

We thank Angelina Vaseva, Ray Phillip Llenes, Stephen D'Amico, Jaime LeBarron, and Rhodora Cristina Calizo, for technical help and Dr. Lucy Skrabanek for helpful discussions. We are grateful to Dr. Elliott Ross for critically reading the manuscript. Computational resources of the David A. Cofrin Center for Biomedical Information in the HRH Prince Alwaleed Bin Talal Bin Abdulaziz Alsaud Institute for Computational Biomedicine are gratefully acknowledged.

**Authorship Contributions**

*Participated in research design:* Scarlata and Weinstein.

*Conducted experiments:* Han, Golebiewska, Stolzenberg, and Scarlata.

*Performed data analysis:* Han, Golebiewska, Stolzenberg, Scarlata, and Weinstein.

*Wrote or contributed to the writing of the manuscript:* Scarlata and Weinstein.

**References**

Bonacci TM, Ghosh M, Malik S, and Smrcka AV (2005) Regulatory interactions between the amino terminus of G-protein betagamma subunits and the catalytic domain of phospholipase Cbeta2. *J Biol Chem* **280:**10174–10181.

Buck E, Li J, Chen Y, Weng G, Scarlata S, and Iyengar R (1999) Resolution of a signal transfer region from a general binding domain in gbeta for stimulation of phospholipase C-beta2. *Science* **283:**1332–1335.

Chen R, Li L, and Weng Z (2003) ZDOCK: an initial-stage protein-docking algorithm. *Proteins* **52:**80–87.

Drin G, Douguet D, and Scarlata S (2006) The pleckstrin homology domain of phospholipase Cbeta transmits enzymatic activation through modulation of the membrane-domain orientation. *Biochemistry* **45:**5712–5724.

Drin G and Scarlata S (2007) Stimulation of phospholipase C[beta] by membrane interactions, interdomain movement, and G protein binding – How many ways can you activate an enzyme? *Cell Signalling* **19:**1383–1392.

Feng J, Roberts MF, Drin G, and Scarlata S (2005) Dissection of the steps of phospholipase C beta 2 activity that are enhanced by G beta gamma subunits. *Biochemistry* **44:**2577–2584.

Gray JJ, Moughon S, Wang C, Schueler-Furman O, Kuhlman B, Rohl CA, and Baker D (2003) Protein-protein docking with simultaneous optimization of rigid-body displacement and side-chain conformations. *J Mol Biol* **331:**281–299.

Guo Y, Golebiewska U, D'Amico S, and Scarlata S (2010) The small G protein Rac1 activates phospholipase C$\delta$1 through phospholipase C$\beta$2. *J Biol Chem* **285:**24999–25008.

Harden TK and Sondek J (2006) Regulation of phospholipase C isoenzymes by ras superfamily GTPases. *Annu Rev Pharmacol Toxicol* **46:**355–379.

Hicks SN, Jezyk MR, Gershburg S, Seifert JP, Harden TK, and Sondek J (2008) General and versatile autoinhibition of PLC isozymes. *Mol Cell* **31:**383–394.

Ilkaeva O, Kinch LN, Paulssen RH, and Ross EM (2002) Mutations in the carboxyl-terminal domain of phospholipase C-beta 1 delineate the dimer interface and a potential Galphaq interaction site. *J Biol Chem* **277:**4294–4300.

Jezyk MR, Snyder JT, Gershberg S, Worthylake DK, Harden TK, and Sondek J (2006) Crystal structure of Rac1 bound to its effector phospholipase C-beta2. *Nat Struct Mol Biol* **13:**1135–1140.

Kozasa T and Gilman AG (1995) Purification of recombinant G proteins from Sf9 cells by hexahistidine tagging of associated subunits. Characterization of $\alpha_{12}$ and inhibition of adenylyl cyclase by $\alpha_z$. *J Biol Chem* **270:**1734–1741.

Lee CW, Lee KH, Lee SB, Park D, and Rhee SG (1994) Regulation of phospholipase C-beta 4 by ribonucleotides and the alpha subunit of Gq. *J Biol Chem* **269:**25335–25338.

Li Y, Sternweis PM, Charnecki S, Smith TF, Gilman AG, Neer EJ, and Kozasa T (1998) Sites for Galpha binding on the G protein beta subunit overlap with sites for regulation of phospholipase Cbeta and adenylyl cyclase. *J Biol Chem* **273:**16265–16272.

Lodowski DT, Pitcher JA, Capel WD, Lefkowitz RJ, and Tesmer JJ (2003) Keeping G proteins at bay: a complex between G protein-coupled receptor kinase 2 and Gbetagamma. *Science* **300:**1256–1262.

London N and Schueler-Furman O (2008) FunHunt: model selection based on energy landscape characteristics. *Biochem Soc Trans* **36:**1418–1421.

Marrink SJ, Risselada HJ, Yefimov S, Tieleman DP, and de Vries AH (2007) The MARTINI force field: coarse grained model for biomolecular simulations. *J Phys Chem B* **111:**7812–7824.

Méndez R, Leplae R, Lensink MF, and Wodak SJ (2005) Assessment of CAPRI predictions in rounds 3–5 shows progress in docking procedures. *Proteins* **60:**150–169.

Panchenko MP, Saxena K, Li Y, Charnecki S, Sternweis PM, Smith TF, Gilman AG, Kozasa T, and Neer EJ (1998) Sites important for PLCbeta2 activation by the G protein betagamma subunit map to the sides of the beta propeller structure. *J Biol Chem* **273:**28298–28304.

Rebecchi M, Peterson A, and McLaughlin S (1992) Phosphoinositide-specific phospholipase C-delta 1 binds with high affinity to phospholipid vesicles containing phosphatidylinositol 4,5-bisphosphate. *Biochemistry* **31:**12742–12747.

Rebecchi MJ and Pentyala SN (2000) Structure, function, and control of phosphoinositide-specific phospholipase C. *Physiol Rev* **80:**1291–1335.

Rebecchi MJ and Scarlata S (1998) Pleckstrin homology domains: a common fold with diverse functions. *Annu Rev Biophys Biomol Struct* **27:**503–528.

Rhee SG (2001) Regulation of phosphoinositide-specific phospholipase C. *Annu Rev Biochem* **70:**281–312.

Runnels LW, Jenco J, Morris A, and Scarlata S (1996) Membrane binding of phospholipases C-beta 1 and C-beta 2 is independent of phosphatidylinositol 4,5-bisphosphate and the alpha and beta gamma subunits of G proteins. *Biochemistry* **35:**16824–16832.

Scarlata S (2002) Determination of the strength and specificity of membrane-bound protein association using fluorescence spectroscopy. *Methods Enzymol* **345:**306–327.

Schneidman-Duhovny D, Inbar Y, Polak V, Shatsky M, Halperin I, Benyamini H, Barzilai A, Dror O, Haspel N, Nussinov R, et al. (2003) Taking geometry to its edge: fast unbound rigid (and hinge-bent) docking. *Proteins* **52:**107–112.

Shan J, Weinstein H, and Mehler EL (2010) Probing the structural determinants for the function of intracellular loop 2 in structurally cognate G-protein-coupled receptors. *Biochemistry* **49:**10691–10701.
Suh PG, Park JI, Manzoli L, Cocco L, Peak JC, Katan M, Fukami K, Kataoka T, Yun S, and Ryu SH (2008) Multiple roles of phosphoinositide-specific phospholipase C isozymes. *BMB reports* **41:**415–434.
van der Meer W, Coker G, and Chen SS(1994) *Resonance Energy Transfer, Theory and Data.* VCH Publishers, Inc., New York.
Van Der Spoel D, Lindahl E, Hess B, Groenhof G, Mark AE, and Berendsen HJ (2005) GROMACS: fast, flexible, and free. *J Comput Chem* **26:**1701–1718.
Wang T, Dowal L, El-Maghrabi MR, Rebecchi M, and Scarlata S (2000) The pleckstrin homology domain of phospholipase C-beta(2) links the binding of Gbetagamma to activation of the catalytic core. *J Biol Chem* **275:**7466–7469.
Wang T, Pentyala S, Rebecchi MJ, and Scarlata S (1999) Differential association of the pleckstrin homology domains of phospholipases C-beta 1, C-beta 2, and C-delta 1 with lipid bilayers and the beta gamma subunits of heterotrimeric G proteins. *Biochemistry* **38:**1517–1524.

**Address correspondence to:** S. Scarlata, Department of Physiology and Biophysics, Stony Brook University, Stony Brook, NY 11794-8661. E-mail: suzanne.scarlata@stonybrook.edu